DOSIMETRIC EVALUATION OF DATA ON THE SOLID ANGLE BREAKDOWN OF SHIELD THICKNESS FOR THE APOLLO VEHICLE

Hermann J. Schaefer

JOINT REPORT

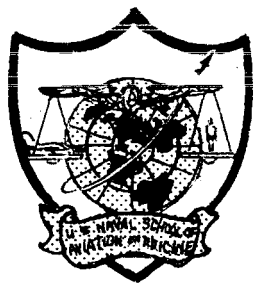

UNITED STATES NAVAL SCHOOL OF AVIATION MEDICINE

NATIONAL AERONAUTICS AND SPACE ADMINISTRATION

Research Report

DOSIMETRIC EVALUATION OF DATA ON THE SOLID ANGLE BREAKDOWN OF SHIELD THICKNESS FOR THE APOLLO VEHICLE

Hermann J. Schaefer

Bureau of Medicine and Surgery
Project MR005.13-1002
Subtask 1 Report No. 29

NASA Order No. R-75

Approved by

Captain Ashton Graybiel, MC USN
Director of Research

Released by

Captain H. C. Hunley, MC USN
Commanding Officer

19 August 1964

U. S. NAVAL SCHOOL OF AVIATION MEDICINE
U. S. NAVAL AVIATION MEDICAL CENTER
PENSACOLA, FLORIDA

SUMMARY PAGE

THE PROBLEM

The Manned Spacecraft Center of NASA has released detailed data of North American Aviation, Inc. on the directional shielding of the Apollo vehicle for a target point in the center of the Command module. These data lend themselves to an evaluation of the radiation exposure for a representative spectrum of flare produced protons. Since shield thickness is distributed randomly, the directional flux components at the target point exhibit an irregular pattern leading to an extremely complex dose distribution in a compact target. It seems useful to set up an equivalent system by rearranging the shield thickness distribution which would allow conclusions to be drawn as to upper and lower limits of the exposure conditions in the actual system.

FINDINGS

It is shown that, by converting the irregularly shaped solid angles of the actual system into ring-shaped sections and arranging them in ascending order of thickness about one axis, an equivalent system of spherical symmetry can be established which furnishes, for a spherical target in its center, the aforementioned upper and lower limit exposure values. Analysis of the exposure in a spherical tissue target of 30 cm diameter in the equivalent system shows that the ratios of percentage contribution to percentage solid angle for absorbed dose and enders count show greatly different depth gradients. Furthermore, the ratio for the enders count for the solid angle of lowest shield thickness shows, for the target surface, the very high value of 5.86, indicating an exceptionally weak link in the entire shield configuration. Since the enders count in the target surface has special significance for the exposure of the lenses of the astronauts' eyes and since the relative position of the astronauts to the sectional solid angle in question is the worst possible, it is suggested that the shield thickness in this section be increased.

The width of variation of absorbed dose and enders count in the target sphere shows strong dependence on depth. In the target surface, variation is maximal and becomes zero in the center. This means that exposure at a fixed point in the surface of the target will change greatly if the target changes orientation in the Command module, but will not change at all in the center. The great variation of absorbed dose and enders count in the target sphere and their strong dependence on a number of parameters concerning orientation and position indicate that accurate measurement of the radiation exposure of the astronauts would require multiple radiation sensors worn on the body.

INTRODUCTION

The Manned Spacecraft Center of NASA has made available data of North American Aviation, Inc. (NAA) on the directional shield thickness distribution in the Apollo vehicle. The data are based on a detailed analysis of the design blueprints of the combined Command and Service modules and furnish, for a target point in the center of the Command module, a breakdown of the 4 pi solid angle into 205 fractional solid angles listing, for the mean direction of arrival of incident radiation, the combined shield thickness of vehicle frame and equipment. Though the literature already contains numerous studies in which tissue dosages from space radiation proton beams behind various fictitious shield configurations have been computed, it seems of definite interest to add to these earlier studies one which pertains to an actual space system. The following report presents the results of such an analysis of the NAA data for a proton energy spectrum that can be considered representative for a large flare event. It investigates the general characteristics of the residual flux at the target point in the Command module as well as the distribution of total absorbed dose and enders count in a 30 cm diameter tissue sphere.

It is quite obvious that, for a space system of such enormous complexity as the Apollo vehicle, equivalent shield thickness varies greatly, exhibiting an extremely irregular directional distribution. As a consequence, the dosage field in a tissue sphere visualized at the target point in the center of the ship can be expected to exhibit a similarly irregular pattern. Aside from the fact that the point by point evaluation of this field would be a very tedious computational venture, such a study would be of little actual value since the results would consist of a pattern of irregularly varying depth dose values with no directional symmetry and certainly would not present a very clear picture of the radiation load. In the present investigation, an attempt has been made to rearrange and order the irregular distribution of shield thickness in such a way that the radiation field within the Command module assumes higher symmetry, yet remains equivalent to the actual field to the extent that it delineates maximum and minimum depth dose curves between which the corresponding dosages in the actual system will always be contained. It is felt that in this way the inherent shielding properties of vehicle and equipment are described more clearly and concisely, allowing comparisons of dose levels with official permissible or critical limits.

REARRANGEMENT OF THE ORIGINAL NAA SOLID ANGLE BREAKDOWN DATA

The original data of NAA are presented in terms of a three-dimensional coordinate system indicated in Figure 1. The full 4 pi space about the center of the Command module is broken down into 205 subsolid angles each one defined individually, with regard to size and orientation, by pairs of zenith and azimuth angles. A

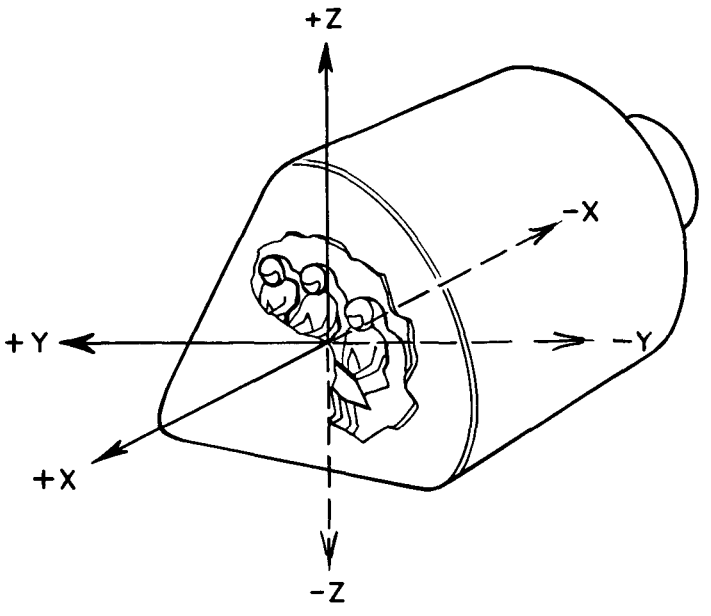

Figure 1

Coordinate System Defining Direction in Relation to Target Point in Command Module of Apollo Vehicle

transcript of the original data, rearranged in order of increasing shield thicknesses and simplified by lumping together solid angles with the same equivalent shield thickness into one item, is presented in Table I* for the anterior hemisphere as seen from the astronaut and in Table II for the posterior hemisphere. Zenith and azimuth angles defining spatial orientation are omitted since they are not needed for the present study; the reasons are explained below. NASA numbers listed in the first column of both tables refer to the original tabulation. Shield thicknesses are given, in the NAA data, to three decimal places in g/cm^2. Quite obviously, for a general estimate of exposure levels, such extreme accuracy is not needed. It seems entirely acceptable to combine solid angles, for which shield thicknesses differ only by a few per cent, into one angle with a weighted mean thickness. This operation has been carried out by treating the data in Tables I and II as one set. Mean thicknesses, in the simplified system, are rounded off to the nearest quarter of a full g/cm^2 because the ionization function for the spectrum to be evaluated was tabulated in steps of $0.25\ g/cm^2$. The original system of 205 sections, already reduced to 101 sections in Tables I and II, is drastically simplified, by the indicated operation, to 18 sections. They are listed, with their respective solid angles and shield thicknesses, in the first three columns of the top part of Table III.

---

* In order not to break the continuity of the text all tables appear at the end of the report.

The orientation in space of the original 205 solid angles as well as those of the simplified system is basically irregular in the sense that shield thickness varies discontinuously and randomly with zenith and azimuth angles. To be sure, by way of a general statement it could be said that radiation incident from the anterior hemisphere for which the positive x axis marks zenith direction encounters, on the average, smaller thicknesses than radiation incident from the posterior hemisphere about the negative x axis for which the huge fuel tanks provide tremendous shielding equivalents subtending quite large solid angles. This general situation is indicated in Figure 2.

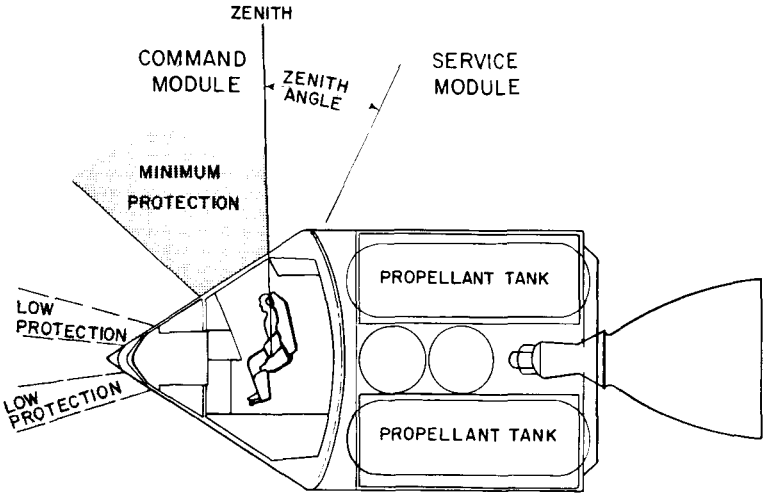

Figure 2

Cross Section of Apollo Vehicle in the X-Z Plane

We propose now to rearrange the randomly distributed sectional solid angles with different shield thickness of the actual system in such a way that an equivalent system is obtained for which the radiation field inside shows a certain symmetry, thereby facilitating the analysis of the depth dose distribution in a target. The principle of this rearrangement may be explained with the aid of the sketches in Figure 3. The left-hand sketch shows a fictitious random distribution of sectional solid angles of five different shield thicknesses forming a spherical shield about a spherical tissue target. It is obvious that the depth dose distribution in the target for omnidirectionally incident radiation will also be irregular. At some point within the solid angle of minimum shield thickness, the surface dose in the target presumably will be at a maximum, although this would depend to some degree on the relative sizes and respective shield thicknesses of the adjacent solid angles. Similarly, minimum surface dose in the target would be expected to occur within the solid angle of heaviest shielding.

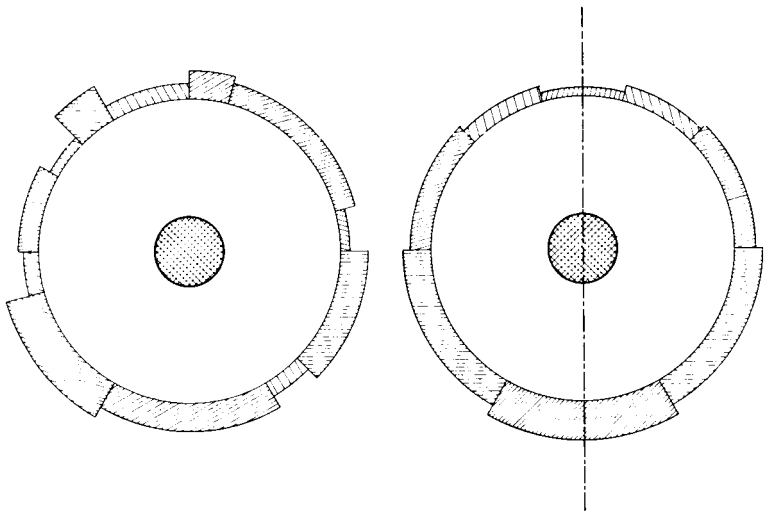

Figure 3

Sketch Explaining Rearrangement
of Shield Thickness Distribution

The left-hand system in Figure 3 is now changed into that shown in the right-nand sketch. An axis of symmetry is assumed as indicated by the vertical dash-dot line. Next, every solid angle of the actual system is changed in shape, but not in size, to a ring-shaped solid angle of constant width centered on the axis of symmetry. All angles are ordered in sequence of increasing thickness, beginning at the zenith of the equivalent system with minimum thickness and ending at the nadir with maximum thickness. It is seen by inspection that in the equivalent system, for omnidirectional irradiation, maximum surface dose in the tissue target will occur for zenith angle zero and minimum surface dose for zenith angle 180° (nadir). At the same time, these two doses are limiting cases that can never be reached at any surface point of the tissue sphere in the actual system. This follows from the fact that, for the zenith point on the target sphere, protons incident from the upper hemisphere suffer minimum attenuation since they encounter minimum thickness in the outer shield and no additional self shielding in the target, whereas for the nadir point on the target sphere the same protons suffer maximum possible self shielding in the target. Any disarrangement in the symmetry of shield thickness distribution as realized in the equivalent system must deteriorate the extreme conditions just formulated; i.e., it will decrease the maximum dose in the zenith point of the target and increase the minimum dose in the nadir point. It is seen, then, that the depth dose distribution along the axis of symmetry through the target sphere begins, in the zenith point, with an upper limit surface dose that will never be fully reached at any

target surface point in the actual system and ends, in the nadir point, with a lower limit surface dose. Furthermore, for obvious geometrical reasons, the depth dose in the center of the target sphere is the same in both systems. In other words, depth doses on the upper half of the symmetry axis represent upper limits and on the lower half lower limits for the infinite variety of depth doses at corresponding radial distances in the actual system.

GENERAL CHARACTERISTICS OF RESIDUAL FLUX IN THE CENTER OF THE COMMAND MODULE

Before the depth dose distribution along the symmetry axis of the target sphere in the equivalent system is established for a typical proton spectrum, some general properties of the residual particle flux in the center of the equivalent system will be investigated. Admittedly, an analysis of the flux within a space vehicle for omnidirectionally incident protons without assuming a specific target such as a human body is not of much practical value since the target, especially in the narrow confines of a smaller ship, would greatly alter the field through absorption effects. However, for the particular system under investigation, such a general analysis would furnish information, for a given proton spectrum, on the contribution of each section to the combined shielding power of the system.

From a dosimetric viewpoint, three magnitudes of the residual flux appear of special significance. The first one naturally would be the total energy, more precisely, the total ionizing power which the flux would develop if totally absorbed in tissue. In official terminology of the ICRU (1), this magnitude is called energy fluence. It is defined as the sum of the energies, exclusive of rest energy, of all the particles which enter a sphere of unit cross-sectional area.

The second magnitude of interest is the exposure dose rate which the residual flux would produce in the center of the Command module, i.e., the dose rate in air as it would be recorded by a small ion chamber. For a unidirectional beam of protons, the exposure dose rate would be directly identical with the dose rate in the surface of a tissue target. Admittedly, this proposition is not correct for omnidirectionally incident radiation as it normally prevails in space. Self shielding effects in the target, in the latter case, would greatly change the dose rate. However, for the particular system under discussion, the proposition of air dose being equal to surface dose does hold for each section considered separately. As seen from Table III, the largest solid angle subtended by any section is that of C14 equalling only 12.7 per cent of 4 pi. That means that, for points on the surface of the target in that section, self shielding effects are negligible for obvious geometrical reasons. In other words, the individual contributions of the various sections to the exposure dose rate represent correctly the respective contributions to local surface dose rates as they would develop in any target.

The third quantity of interest is the number of "enders" per unit tissue volume, i.e., of protons reaching the end of their ionization range. The density of enders in tissue directly determines the fraction of the total ionization dosage that is produced at a high linear energy transfer (LET) and that would accordingly have a relative biological effectiveness (RBE) greater than 1.0. Here again, it seems of interest to identify the individual contribution from each section in view of the fact that the enders count and exposure dose show different dependences on shield thickness.

An explanation seems in order concerning the unit for expressing the number of enders. At first sight, it might seem preferable to express the enders count in terms of absorbed energy per gram tissue, i.e., in rads. However, this would require an agreement on the residual range for which the energy dissipation from enders is to be considered. This residual range, in turn, would depend on the critical LET or kinetic energy which one would select for defining LET as high. In terms of official recommendations of the ICRP (2) this would mean an agreement on the corresponding critical RBE and QF factors. Table IV lists a number of choices for these factors, together with their corresponding energies and LET values. The last column shows absorbed doses in microrads for 1,000 enders per gram tissue. Actually, a specific value above which LET is to be considered high as compared to standard x-rays cannot be defined since a number of criteria leading to different values in the general range from about 10 to about 50 kev/micron$_T$ could be chosen. This author has selected, in an earlier study (3), the upper energy limit of 0.5 Mev corresponding to an LET of 40 kev/micron$_T$ for assessing the high LET fraction of the total ionization dose from protons. This is basically an arbitrary choice, and it might be preferable to express the phenomenon of protons ending in tissue directly by the number per unit mass of tissue as long as no specific biologic effects are considered.

The proton spectrum selected for evaluation in the present study is the one proposed by Bailey (4) as representative for a large flare event. More recently, Freier and Webber (5) have evaluated six large flare events of the past solar maximum and described their momentum spectra by a general exponential expression. However, flux values for individual flare events are defined only for limited sections of the total interval of momenta that would be of interest for evaluation of exposure. Quite differently, Bailey's "synthetic" spectrum covers the entire momentum range of interest from a dosimetric viewpoint. A comparison shows that Bailey's spectrum delineates very satisfactorily the upper envelope of Freier and Webber's group of typical spectra if they are transformed into energy spectra. Bailey's spectrum, then, seems a good choice for obtaining comprehensive information on maximum flare dose rates with the only limitation that the exceptionally rare type of a so-called relativistic flare with strong flux values up to and beyond 1 Bev would not be included.

Table III also presents data on the residual flux for the 18 sections of the equivalent system for Bailey's flare spectrum. It is of special interest to compare the

percentage contributions from individual sections to their percentage solid angles. The pertinent ratios are listed in the lower part of Table III in the last three columns. It is seen that, for all three magnitudes, energy fluence, total dose, and enders count, the quotients start, at low shield thickness, with values substantially larger than 1.0, then drop to 1.0 at some medium heavy thickness, and end up with values substantially smaller than 1.0 at high shield thickness. Basically, this is a trivial finding as it indicates merely that heavily shielded solid angles contribute smaller intensities than lighter ones. However, it seems of special interest that the three dosimetric magnitudes reach a point of balance at which the percentage contribution becomes equal to the percentage solid angle at different shield thicknesses. For the energy fluence, the point is reached at about 10 g/cm^2 (Sections C8 and C9), for the exposure dose rate at 8 g/cm^2 (Sections C6 and C7), and for the enders count as soon as 6.75 g/cm^2. Furthermore, the extremely large ratio of 5.86 for the enders count at the lightest shield thickness (C1; 1.75 g/cm^2) is noteworthy. It is indicative of the fact that the enders count shows throughout a substantially larger depth gradient than energy fluence and exposure, a circumstance which illustrates how difficult it is to furnish a complete dosimetric analysis of the residual flux.

DEPTH DOSE DISTRIBUTION IN A SPHERICAL TISSUE TARGET IN THE COMMAND MODULE

The quantitative analysis has been carried out by numerical integration of absorbed dose and enders count along the vertical diameter in a target sphere in the center of the equivalent system for Bailey's model spectrum. For this purpose, the 18 sections of the equivalent system were further subdivided into a total of 25 sections. This was done to achieve higher accuracy since each section was to be represented by one value of combined thickness of shield and target for the mean direction of arrival of protons. For each of 29 selected points on the vertical diameter the 25 contributions to total dose and enders count were added and the sums plotted. The resulting graphs are presented in Figure 4. It is seen that the absorbed dose drops from a sharp maximum of 1.27 rads/hour in the upper surface point of the target sphere to a flat minimum of 0.23 rads/hour in the lower half of the target sphere and then slightly recovers to 0.45 rads/hour in the lower surface point. The corresponding values for the enders count are 282, 28, and 68 enders/sec gram$_T$. For conversion of enders count values into millirads, Table IV should be consulted.

As explained in the preceding section, the upper and lower halves of the two depth distributions for total dose and enders count represent the upper and lower limits for the same magnitudes at corresponding points on radii of any direction in the actual system. It is, therefore, of better descriptiveness to align, on one depth scale as abscissa, the upper and lower halves of the distribution, as shown in Figure 5. The curves now directly delineate areas of possible doses or enders counts in the actual system, i.e., in a tissue sphere in the center of the Command module.

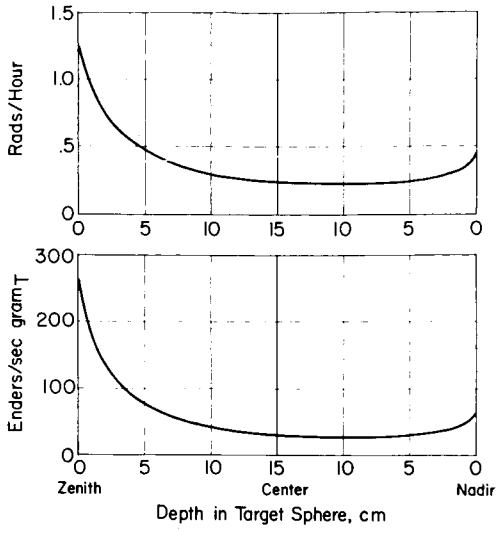

Figure 4

Depth Distribution of Total Absorbed Dose and Enders Count in Tissue Sphere of 30 cm Diameter at Center of Equivalent System for Bailey's Flare Spectrum

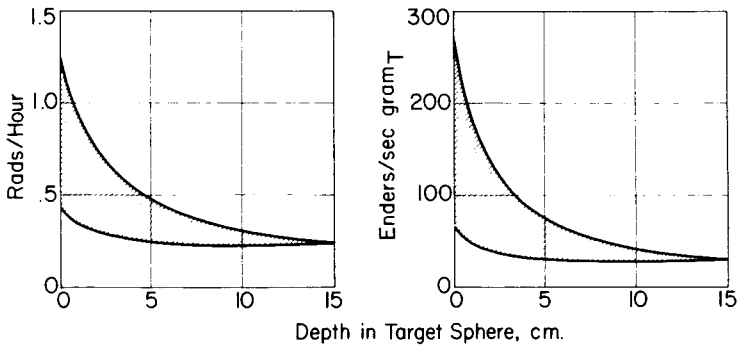

Figure 5

Graphs of Figure 4 Folded Over for Showing Width of Variation of Dose and Enders Count in Tissue Sphere at Target Point in Command Module

The graphs in Figures 4 and 5 indicate that the enders count drops off more steeply toward greater depths and reaches a smaller minimum than the total dose. For a quantitative comparative evaluation of this relationship, it is necessary to normalize distributions to equal surface values. The result of this transformation is shown in Figure 6. Steeper drop and lower minimum of the enders count can now be compared directly and quantitatively to the total dose. It is seen that the difference in the depth distribution of dose and enders count is indeed substantial. The reason for the much steeper gradient of the enders count rests in the fact that the enders count, at a given point in the target, is due to protons from a sharply limited energy interval in the differential energy spectrum of the incident beam, whereas the total absorbed dose at the same point is due to the protons of all energies from the absorption cutoff at that point on to infinity. That means the total absorbed dose is partly produced by particles of high and very high energies which show little attenuation and therefore produce a smaller depth gradient.

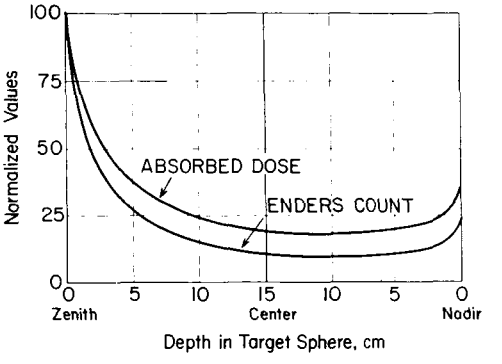

Figure 6

Data of Figure 4 Normalized to Equal Surface Values at Zenith Point Showing Greater Depth Gradient and Lower Minimum of Enders Count

DISCUSSION

If we proceed to discuss the significance of the foregoing evaluation for the radiation exposure of the astronaut, it would be obvious that the spatial arrangement of material and equipment in the Apollo vehicle, which has lead to the characteristic shield distribution of the actual and equivalent system, is dictated by design requirements not at all connected with the radiation safety issue. Therefore, a discussion of how this spatial arrangement could be changed for optimization or at least improvement of effective shielding power seems unrealistic. Merely in one instance, such a change might be proposed. It concerns the extremely high peak

of the enders count in the target surface for section C1, that of lowest shield thickness marked in Figure 2 with "Minimum Protection." A high enders count in the surface of a human target has particular significance for the lenses of the eyes for which official radiation safety rules are especially stringent. It is evident that the relative positions of the astronauts and of shield section C1 combine toward the worst possible conditions as far as exposure of the lenses of the eyes is concerned. Whether a protective visor or a general increase of shield thickness in section C1 is the more adequate way of strengthening this weak spot is not to be decided here. The essential point is that section C1 is of disporportionately lower shielding power than even the next higher section and that only a moderate weight penalty would have to be accepted for achieving substantial improvement.

Another interesting feature of the depth dose distribution in the target sphere is the changing vertical width of the shaded areas in Figure 5. As pointed out in the preceding section, this width directly indicates the variation of exposure values at corresponding points for the target sphere in the actual system, i.e., in the Command module. It is seen that this variation is maximal for the surface point and narrows as the center of the target sphere is approached. In the center itself, the variation is zero, indicating that exposure conditions in the actual and equivalent system are identical. Expressed differently, this relationship means that changes in exposure that occur in a fixed point in the target sphere when it changes its orientation in the Command module will be maximal if this point is in the surface and will be zero in the center. Though this proposition cannot be transferred directly to a target of such complicated geometrical configuration as a human body, it still holds to the extent that in such a target, as it changes its orientation in the Command module, exposure will change maximally in the surface and more moderately in deeper regions.

Much greater alterations of the dose distribution will occur if not only a change of orientation, but also actual locomotion of the target in the Command module takes place because in that case the solid angles and equivalent shield thicknesses themselves would change. This is additional evidence demonstrating the infinitely complex ever changing structure of the radiation field inside the ship. Equally complex is the task of designing a system of multiple radiation sensors to be worn by the astronaut, simple and light enough not to overburden him, yet elaborate enough to allow accurate assessment of the total body radiation load.

REFERENCES

1. International Commission on Radiological Units and Measurements (ICRU), Radiation quantities and units. Report 10a. Handbook 84. Washington, D. C.: National Bureau of Standards, 1962.

2. Report of the RBE Committee to the International Commissions on Radiological Protection and on Radiological Units and Measurements. Health Physics, 9:357-384, 1963.

3. Schaefer, H. J., LET analysis of tissue ionization dosages for proton radiations in space. BuMed Project MR005.13-1002 Subtask 1, Report No. 21. Pensacola, Fla.: U. S. Naval School of Aviation Medicine, 1962.

4. Bailey, D. K., Abnormal ionization in the lower ionosphere associated with cosmic-ray flux enhancements. Proc. I.R.E., 47:255-266, 1959.

5. Freier, P. S., and Webber, W. R., Exponential rigidity spectrums for solar-flare cosmic rays. J. Geophys. Res., 68:1605-1629, 1963.

Table I

Distribution of Shield Thickness in Center of Command Module for Anterior Hemisphere as Seen From Astronaut

NASA No.	Solid Angle, steradians	Shield Thickness, g/cm^2	NASA No.	Solid Angle, steradians	Shield Thickness, g/cm^2
197	.01711	1.676	173,174	.06836	9.462
141-143			189,190	.03802	9.909
148-150	.93798	1.81	187,188	.10549	10.455
155-157			159	.38144	10.519
198-201	.09148	3.569	185,186	.08078	10.693
193,194	.01900	3.583	171	.22900	10.935
202-205	.02392	4.121	172	.06152	10.994
191,192	.01900	4.231	164,165	.08037	12.771
170	.09119	4.964	175	.20165	13.237
195,196	.06272	5.736	166-169	.22258	13.859
161-163	.16230	7.077	134,135	.22438	13.925
139,140			160	.20194	15.316
145-147	.28362	7.38	178,179	.06836	15.498
153,154			184	.06152	15.895
138,152	.12464	7.656	183	.11621	17.567
137	.22438	8.409	182	.06152	17.788
136	.43753	8.479	176,177	.13672	21.951
144			180,181	.22556	21.959
151	.26926	8.524	133	.20194	27.768
158			132	.75166	27.899

Table II

Distribution of Shield Thickness in Center of Command Module for Posterior Hemisphere as Seen From Astronaut

NASA No.	Solid Angle, steradians	Shield Thickness, g/cm^2	NASA No.	Solid Angle, steradians	Shield Thickness, g/cm^2
125,126	.14455	3.57	28-39	.01824	19.906
53-58	.00580	4.99	113	.04574	21.864
72-74	.07905	5.185	40	.00429	21.996
69-71	.07905	5.416	98	.19154	23.289
123,124	.04518	5.442	112	.06861	24.852
107,108	.09148	5.619	117	.08131	26.471
76	.19759	6.1	104	.04574	27.852
96,97	.23639	6.412	102	.11150	28.954
88	.12946	6.655	90,91	.22361	29.012
79	.10788	6.993	114	.05146	29.034
67,68	.39398	7.0	103	.05718	31.444
80,81	.30207	7.141	116	.30206	35.27
65,66	.45964	7.216	13-16	.02288	37.484
105,106	.02858	7.492	17-20	.00753	38.311
78	.16788	8.194	59,75	.05517	41.2
127,128	.28007	8.294	9-12	.00860	42.744
85-87	.04312	8.713	21,22	.00502	50.875
122	.07228	8.877	46	.01850	56.76
82-84	.04314	9.027	41	.00429	60.036
109,110	.12579	9.739	63,64	.08024	64.0
131	.08131	10.48	48	.01030	68.9
120	.17617	10.698	42,43	.01030	74.0
100,101	.05718	11.567	23	.00179	84.709
129	.10841	11.658	60	.02174	91.76
121	.09035	11.886	61,62	.09362	98.20
115	.05146	12.524	47	.00898	108.1
89	.12946	14.280	5-8	.01148	110.494
92,93	.02556	14.32	1-4	.00384	113.914
94,95	.28112	14.508	44,45	.01200	119.0
77	.16416	14.54	49,50	.05218	155.5
118,119	.09034	14.552	24,25	.04440	182.3
130	.15359	15.64	26,27	.05178	214.0
111	.05146	15.869	51,52	.06088	261.0
99	.05415	18.107			

Table III

Energy Fluence, Exposure Dose Rate, and Enders Count
in Center of Command Module for Bailey's Flare Spectrum

Solid Angle, Navy No.	Solid Angle, steradians	Shield Thickness, g/cm^2	Energy Fluence, $Mev/(sec\ cm^2)$	Exposure Dose Rate, milliroentgens per hour	Enders Count, $N/(sec\ gram_T)$
C1	0.955	1.75	43,077	429.1	134.7
C2	0.298	3.5	10,534	77.84	17.28
C3	0.470	5.25	13,699	85.24	17.16
C4	0.564	6.5	14,556	82.60	14.83
C5	1.292	7.0	31,865	176.0	30.88
C6	0.571	7.5	13,473	72.1	12.50
C7	1.038	8.5	22,506	114.0	19.83
C8	0.672	8.75	14,282	71.8	12.43
C9	0.804	10.75	14,586	68.1	11.50
C10	0.565	11.25	9,867	45.2	7.57
C11	1.109	14.25	15,651	60.8	9.87
C12	0.949	15.0	12,768	47.2	7.59
C13	0.799	21.0	7,825	22.4	2.81
C14	1.593	28.0	11,446	27.2	3.329
C15	0.397	38.0	1,976	3.44	0.369
C16	0.130	62.0	379.9	0.392	0.0306
C17	0.151	102.0	252.9	0.152	0.0091
C18	0.209	212.0	151.5	0.0654	0.0018

Table III - Continued

Solid Angle, Navy No.	Solid Angle, Per Cent of Total	Energy Fluence, Per Cent of Total	Exposure Dose Rate, Per Cent of Total	Enders Count, Per Cent of Total	% Energy Fluence / % Solid Angle	% Exposure Dose Rate / % Solid Angle	% Enders Count / % Solid Angle
C1	7.600	18.03	31.0	44.5	2.372	4.079	5.855
C2	2.371	4.409	5.625	5.71	1.860	2.370	2.408
C3	3.740	5.734	6.16	5.67	1.533	1.647	1.516
C4	4.488	6.093	5.97	4.90	1.358	1.330	1.092
C5	10.28	13.34	12.7	10.20	1.298	1.235	0.992
C6	4.544	5.640	5.21	4.13	1.241	1.147	0.909
C7	8.260	9.421	8.24	6.55	1.141	0.998	0.793
C8	5.348	5.978	5.19	4.11	1.118	0.970	0.769
C9	6.398	6.106	4.92	3.80	0.954	0.769	0.594
C10	4.496	4.130	3.27	2.50	0.919	0.727	0.556
C11	8.825	6.551	4.39	3.26	0.742	0.497	0.369
C12	7.552	5.345	3.41	2.51	0.708	0.452	0.332
C13	6.358	3.275	1.62	0.928	0.515	0.255	0.156
C14	12.68	4.791	1.97	1.100	0.378	0.155	0.0868
C15	3.159	0.8271	0.249	0.122	0.262	0.0788	0.0386
C16	1.035	0.1590	0.028	0.010	0.154	0.0271	0.0097
C17	1.202	0.1059	0.011	0.003	0.0881	0.0092	0.0025
C18	1.663	0.06342	0.0047	0.00059	0.0381	0.0028	0.00035

Table IV

Relation Between Enders Count in Tissue and
Absorbed Dose for Selected Values of RBE and QF

RBE	QF	Kinetic Energy, Mev	LET, Kev/micron$_T$	Absorbed Dose for 1,000 Enders/gram$_T$, microrads
1.0	1.1	23.4	2.00	415.0
1.5	2.65	2.35	11.8	41.7
2.0	4.2	0.970	21.8	17.2
3.0	7.5	0.483	41.9	8.57
5.0	13.9	0.216	81.7	3.83
0.915	1.0	40.6	1.28	720.0
1.12	1.5	8.70	4.4	154.0
1.28	2.0	4.37	7.5	77.6
1.61	3.0	1.83	14.0	32.5
2.24	5.0	0.740	26.7	13.1
4.80	10.0	0.353	57.8	6.26